Modeling and Simulation of Flight Dynamics of Variable Mass Systems

Marco B. Quadrelli[1], Jonathan Cameron[2], Bob Balaram[3], Mayank Baranwal[4], Alessandro Bruno[5]

Jet Propulsion Laboratory, California Institute of Technology, 4800 Oak Grove Drive, Pasadena, CA 91109-8099

This paper derives the equations of motion of variable mass systems using a coordinate-free approach. These equations have been verified with simple models, and the terms originating in the steady and unsteady gas-dynamic interaction effects have been used in the modeling and simulation of the propulsive phase of the Supersonic Inflatable Advanced Decelerator when the vehicle is spinning. The variable mass terms have an effect both the translation and the rotation of the vehicle during thrust, indicating an increase in the roll rate.

I. Introduction

THE objective of this paper is to describe the modeling and simulation of the flight mechanics of variable mass systems. The models derived in this paper apply to both rigid and flexible variable mass bodies, however this paper is limited to the dynamics of rigid bodies with variable mass. One application is the modeling of the flight dynamics effects on the Supersonic Inflatable Aerodynamic Decelerator (SIAD) during the propulsive phase where the torques arising during the STAR-48 solid motor burn are important.

The equations of motion of variable mass systems are not new[3,4,5,6,7,10,11,12], however a coordinate-free derivation that can be specialized to different cases is new. More specifically, the derivations presented in this paper were motivated by the fact that previous analyses of variable mass systems under thrust are limited to prolate vehicles (rockets). The SIAD vehicle is an oblate vehicle, and the question arose if the same analytical description of the motion, as well as conclusions on the physics of rockets, would apply.

This paper is divided as follows. First, the dynamics of an extended body with variable mass flow is derived. These equations are then validated analytically with the canonical example of a double pendulum. Then, the equations are also compared with previous work on variable mass systems. Second, these equations are applied to the dynamics of a variable mass spinning system under thrust, using the properties of the SIAD vehicle. This analysis includes both steady and unsteady gas-dynamic interaction effects. Finally, a brief discussion is provided on the JPL in-house flight dynamics simulator DSENDS (Dynamic Simulation for Entry, Descent, and Landing Simulator) and its advanced visualization capabilities. The section on conclusions ends the paper.

II. Dynamics of Extended Body with Variable Mass Flow

In this section we derive the equations of motion of a extended body with variable mass flow. To do this, first we recollect the basic ideas behind the Reynold's transport theorem, then we outline the elements of the extended body kinematics and kinetics, and derive the linear and angular momentum balance in coordinate-free form. The equations of motion are validated with a simple, and well-known, double-pendulum example. Finally, these equations are compared to similar equations derived by other authors.

---

[1] Research Technologist, Mobility and Robotic Systems Section, M.S. 198-209, and Senior AIAA Member.
[2] Research Technologist, Mobility and Robotic Systems Section, M.S. 198-209.
[3] Research Technologist, Mobility and Robotic Systems Section, M.S. 198-209.
[4] Graduate Student, University of Illinois at Urbana-Champaign.
[5] Graduate Student, Scuola Superiore Sant'Anna, University of Pisa, Italy.

A. Reynolds Transport Theorem

Reynolds' Transport Theorem is a fundamental theorem used in formulating the basic laws of moving solids or fluids systems[8]. Reynold's transport theorem states that the rate of change of an extensive property N for the system is equal to the time rate of change of N within the control volume and the net rate of flux of the property N through the control surface. This fundamental theorem has two forms:

- Form A

$$\left(\frac{dN}{dt}\right)_{CMS} = \frac{\partial}{\partial t}\iiint_{CV}\eta\rho d\forall + \iint_{CS}\eta\rho(\underline{w}.\underline{dA}) \qquad (1)$$

- Form B

$$\left(\frac{dN}{dt}\right)_{CMS} = \iiint_{CV}\frac{\partial}{\partial t}\eta\rho d\forall + \iint_{CS}\eta\rho(\underline{v}.\underline{dA}) \qquad (2)$$

where,

    N is any fluid property
    η is fluid property per unit mass
    $d\forall$ is differential volume element
    CMS is Control Mass System
    CV is Control Volume
    CS is Control Surface
    $\underline{w}$ is efflux velocity, relative to control surface
    $\underline{v}$ is local material velocity
    If $\underline{v}_{CS}$ is local control surface velocity, then $\underline{v} = \underline{v}_{CS} + \underline{w}$

Note: The two forms are equivalent and state the same law in different forms. One can easily see that if the control surface is non-deforming/rigid, $\underline{v}_{CS} = \underline{0}$, and the derivative in Form A can be taken inside, i.e.,

$$\frac{\partial}{\partial t}\iiint_{CV}\eta\rho d\forall = \iiint_{CV}\frac{\partial}{\partial t}\eta\rho d\forall \qquad (3)$$

B. Continuity Equation

Continuity equation refers to mass conservation equation. Mass conservation principle states that the rate of increase of mass inside the control volume is equal to the net influx through the control surface. Since mass is constant for a CMS (control mass system), using equation 19 and substituting $N = m$ for the extensive fluid property, we can write:

$$0 = \frac{\partial}{\partial t}\int_{CV}\rho \, d\forall + \int_{CS}\rho(\underline{w}.\underline{dA}) \qquad (4)$$

If we denote the rate of change of mass inside the CV by $\dot{m}$, then using equation 22 we can write:

$$\dot{m} = -\int_{CS}\rho(\underline{w}.\underline{dA}) \qquad (5)$$

C. Body Kinematics

Figure 1 shows a body (or a CV) with origin of the body-fixed frame located at point O on the body. The origin of the inertial frame is located at a point O'. At any instant, the position vector of a point on the body in the body-fixed frame is $\underline{r}$. Also, $\underline{R}$ is the location of the origin of the body frame from the origin of the inertial frame. If $\underline{r}'$ is the position vector of the same point in the inertial frame, we can write:

$$\underline{r}' = \underline{R} + \underline{r} + \underline{u} \qquad (6)$$

where u is a body deformation. For simplicity, in this paper we only consider rigid displacements, and u=0. Now, we define the following quantities:

$\underline{\omega}$: angular velocity of the body frame

$\underline{\dot{\omega}}$: angular acceleration of the body frame

$\dfrac{d'}{d't}$: derivative in the inertial frame

$\dfrac{d}{dt}$: derivative in the body frame

$\dfrac{d'\underline{R}}{d't} = \underline{v}_O$: velocity of the origin of the body frame

$\dfrac{d'^2\underline{R}}{d't^2} = \underline{a}_O$: acceleration of the origin of the body frame

$\dfrac{d\underline{r}}{dt} = \underline{v}$: velocity of the particle as observed in the body frame

$\dfrac{d^2\underline{r}}{dt^2} = \underline{a}$: acceleration of the particle as observed in the body frame
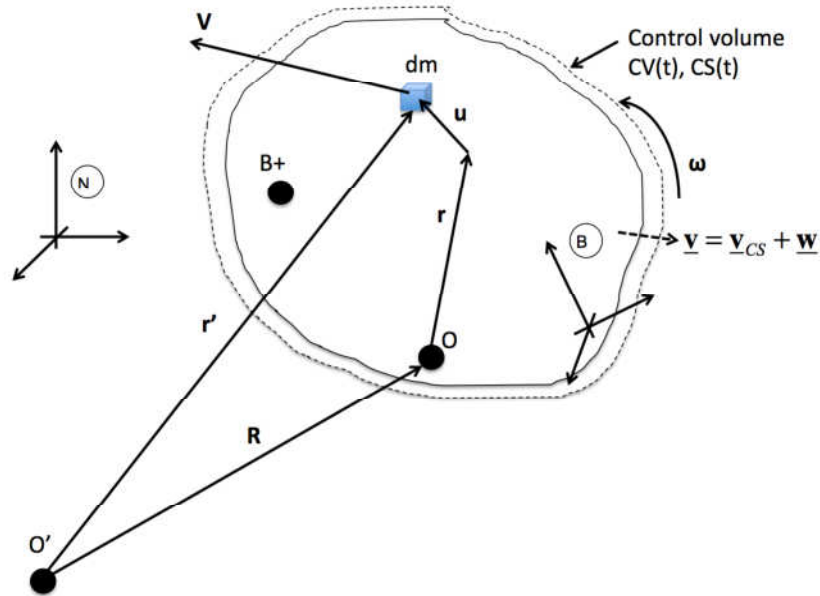
Figure 1. Control volume under mass flow.

Using the basic kinematics of the moving (rotating+translating) frames, we derive the linear velocity and linear acceleration of the generic point as:

$$\frac{d'\underline{r}'}{d't} = \underline{v}_O + \underline{\omega} \times \underline{r} + \frac{d\underline{r}}{dt} \qquad (7)$$

American Institute of Aeronautics and Astronautics

$$\frac{d'^2\underline{r}'}{d't^2} = \underline{a}_O + \underline{\dot{\omega}} \times \underline{r} + \underline{\omega} \times (\underline{\omega} \times \underline{r}) + 2\left(\underline{\omega} \times \frac{d\underline{r}}{dt}\right) + \frac{d\underline{v}}{dt} \tag{8}$$

Correspondingly, the linear momentum of the extended body is:

$$\begin{aligned}
\underline{P} &= \int_{\mathbf{B}} \underline{v}\, dB \\
&= \int_{\mathbf{B}} \left(\underline{v_0} + \underline{\omega} \times \underline{r} + \underline{v}\right) dB \\
&= \underline{v_0}\int_{\mathbf{B}} dB + \int_{\mathbf{B}} \underline{v}\, dB + \underline{\omega} \times \int_{\mathbf{B}} \underline{r}\, dB
\end{aligned}$$

$$\tag{9}$$

and the angular momentum of the extended body about the reference point O is:

$$\begin{aligned}
\underline{H}_o &= \int_{B} \underline{r} \times \underline{v}\, dB \\
&= \int_{B} \underline{r} \times \left(v_0 + \underline{\omega} \times \underline{r} + \underline{v}\right) dB \\
&= -\underline{v}_0 \times \int_{B} \underline{r}\, dB + \int_{B} \underline{r} \times \left(\underline{\omega} \times \underline{r}\right) dB + \int_{B} \underline{r} \times \underline{v}\, dB \\
&= -\underline{v}_0 \times \underline{c} + \int_{B} \underline{r} \times \left(\underline{\omega} \times \underline{r}\right) dB + \int_{B} \underline{r} \times \underline{v}\, dB \\
&= -\underline{v}_0 \times \int_{B} \underline{r}\, dB + \underline{\underline{J}}_0 \cdot \underline{\omega} + \int_{B} r \times \underline{v}\, dB
\end{aligned}$$

$$\tag{10}$$

D. Linear Momentum Balance

Newton's Equation is essentially the linear momentum balance equation. According to linear momentum conservation principle, the net external force on a system is equal to the rate of change of the linear momentum of that system. Substituting N with linear momentum for the extensive fluid property in the Reynold's theorem, we have:

$$\underline{F}_B + \underline{F}_S = \left(\frac{d'}{d't}\int \underline{\dot{r}}'\, dm\right)_{CMS} \tag{11}$$

where, $\underline{F}_B$ is the net external Body Force and $\underline{F}_S$ is the net external Surface Force.

Since the mass is constant for a (CMS) Control Mass System, we can take the derivative inside the integral in the equation 27.

4
American Institute of Aeronautics and Astronautics

$$\underline{F}_B + \underline{F}_S = \left(\int \frac{d'\dot{\underline{r}}'}{d't} \, dm \right)_{CMS} \tag{12}$$

Using the kinematics, we have:

$$\underline{F}_B + \underline{F}_S = \int_{CV} \{ \underline{a}_O + \dot{\underline{\omega}} \times \underline{r} + \underline{\omega} \times (\underline{\omega} \times \underline{r}) \} dm + 2\underline{\omega} \times \left(\int \frac{d\underline{r}}{dt} \, dm \right)_{CMS} + \left(\int \frac{d\underline{v}}{dt} \, dm \right)_{CMS} \tag{13}$$

Now, using Reynold's theorem,

$$\left(\int \frac{d\underline{r}}{dt} \, dm \right)_{CMS} = \frac{d}{dt} \left(\int \underline{r} \, dm \right)_{CMS} \qquad [\because system\ mass\ is\ constant]$$

$$= \frac{\partial}{\partial t} \int_{CV} \rho \underline{r} \, d\forall + \int_{CS} \rho \underline{r}(\underline{w}.\underline{dA}) \tag{14}$$

Similarly,

$$\left(\int \frac{d\underline{v}}{dt} \, dm \right)_{CMS} = \frac{\partial}{\partial t} \int_{CV} \rho \underline{v} \, d\forall + \int_{CS} \rho \underline{v}(\underline{w}.\underline{dA}) \tag{15}$$

Since at any instant, particle velocity $\underline{v}$ is $\frac{d\underline{r}}{dt}$, using Transport Theorem equation (13) can be re-written as:

$$\left(\int \frac{d\underline{v}}{dt} \, dm \right)_{CMS} = \frac{\partial^2}{\partial t^2} \int_{CV} \rho \underline{r} \, d\forall + \frac{\partial}{\partial t} \int_{CS} \rho \underline{r}(\underline{w}.\underline{dA}) + \int_{CS} \rho \underline{v}(\underline{w}.\underline{dA}) \tag{16}$$

Hence, the linear momentum balance for a general variable mass system is:

$$\underline{F}_B + \underline{F}_S = \int_{CV} \rho \{ \underline{a}_O + \dot{\underline{\omega}} \times \underline{r} + \underline{\omega} \times (\underline{\omega} \times \underline{r}) \} d\forall$$

$$+ \underbrace{2\underline{\omega} \times \left(\frac{\partial}{\partial t} \int_{CV} \rho \underline{r} \, d\forall + \int_{CS} \rho \underline{r}(\underline{w}.\underline{dA}) \right)}_{-\underline{F}_C, Coriolis\ Force}$$

$$+ \underbrace{\frac{\partial^2}{\partial t^2} \int_{CV} \rho \underline{r} \, d\forall + \frac{\partial}{\partial t} \int_{CS} \rho \underline{r}(\underline{w}.\underline{dA}) + \int_{CS} \rho \underline{v}(\underline{w}.\underline{dA})}_{-\underline{F}_{rel}, Transport\ Theorem\ in\ Rotating\ Frame}$$

$$\tag{17}$$

E. Angular Momentum Balance

Once we have derived the linear momentum balance, we use a similar approach to derive the angular momentum balance equation. Let us first define the angular momentum about the origin of the inertial frame.

$$\underline{H} = \int \rho(\underline{r}' \times \dot{\underline{r}}') d\forall \tag{18}$$

By substituting the extensive fluid property N with angular momentum about O' in the equation of the Reynold's theorem, we obtain:

$$\sum \underline{M} = \frac{d'}{d't}\left(\int \rho(\underline{r}' \times \underline{\dot{r}}')d\forall\right)_{CMS}$$

$$= \underbrace{\left(\int \rho(\underline{\dot{r}}' \times \underline{\dot{r}}')d\forall\right)_{CMS}}_{0} + \left(\int \rho\left(\underline{r}' \times \frac{d'\underline{\dot{r}}'}{d't}\right)d\forall\right)_{CMS}$$

$$= \underline{R} \times \left(\int \rho \frac{d'\underline{\dot{r}}'}{d't}d\forall\right)_{CMS} + \left(\int \rho\left(\underline{r} \times \frac{d'\underline{\dot{r}}'}{d't}\right)d\forall\right)_{CMS} \quad [from\ equation\ ]$$

$$= \underline{R} \times (\underline{F}_B + \underline{F}_S) + \int_{CV} (\underline{r} \times [\underline{a}_O + \underline{\dot{\omega}} \times \underline{r} + \underline{\omega} \times (\underline{\omega} \times \underline{r})])dm$$

$$+ \left(\int \left(\underline{r} \times 2\underline{\omega} \times \frac{d\underline{r}}{dt}\right)dm\right)_{CMS} + \left(\int \left(\underline{r} \times \frac{d\underline{v}}{dt}\right)dm\right)_{CMS} \quad (19)$$

Using some basic vector algebra, it can be shown:

$$\left(\int \left(\underline{r} \times 2\underline{\omega} \times \frac{d\underline{r}}{dt}\right)dm\right)_{CMS} = \left(\int \frac{d}{dt}(\underline{r} \times \underline{\omega} \times \underline{r})dm\right)_{CMS}$$

$$- \int_{CV} (\underline{r} \times \underline{\dot{\omega}} \times \underline{r})\,dm - \underline{\omega} \times \left(\int \left(\frac{d\underline{r}}{dt} \times \underline{r}\right)dm\right)_{CMS} \quad (20)$$

Hence, from equations 19 and 35, we have:

$$\left(\int \left(\underline{r} \times 2\underline{\omega} \times \frac{d\underline{r}}{dt}\right)dm\right)_{CMS} = \frac{\partial}{\partial t}\underbrace{\int_{CV} \rho(\underline{r} \times \underline{\omega} \times \underline{r})d\forall}_{\underline{I}_O \cdot \underline{\omega}} - \underbrace{\int_{CV} \rho(\underline{r} \times \underline{\dot{\omega}} \times \underline{r})d\forall}_{\underline{I}_O \cdot \underline{\dot{\omega}}}$$

$$+ \int_{CS} \rho(\underline{r} \times \underline{\omega} \times \underline{r})(\underline{w} \cdot \underline{dA}) + \underline{\omega} \times \left(\int_{CV} \rho\left(\underline{r} \times \frac{d\underline{r}}{dt}\right)d\forall\right) \quad (21)$$

where, $\underline{I}_O$ is the moment of inertia tensor of the body about O.

Similarly, the last term in the equation (17) can be re-written as:

$$\left(\int \rho\left(\underline{r} \times \frac{d\underline{v}}{dt}\right)d\forall\right)_{CMS} = \left(\int \rho\frac{d}{dt}(\underline{r} \times \underline{v})d\forall\right)_{CMS} \quad [\because (\underline{v} \times \underline{v}) = \underline{0}]$$

$$= \frac{\partial}{\partial t}\int_{CV} \rho(\underline{r} \times \underline{v})d\forall + \int_{CS} \rho(\underline{r} \times \underline{v})(\underline{w} \cdot \underline{dA}) \quad (22)$$

Also, we list the following quantities:

$$\int_{CV} \rho(\underline{r} \times \underline{\dot{\omega}} \times \underline{r})d\forall = \underline{I}_O \cdot \underline{\dot{\omega}} \quad (23)$$

$$\int_{CV} \rho(\underline{r} \times \underline{\omega} \times \underline{\omega} \times \underline{r})d\forall = \underline{\omega} \times (\underline{I}_O \cdot \underline{\omega}) \quad (24)$$
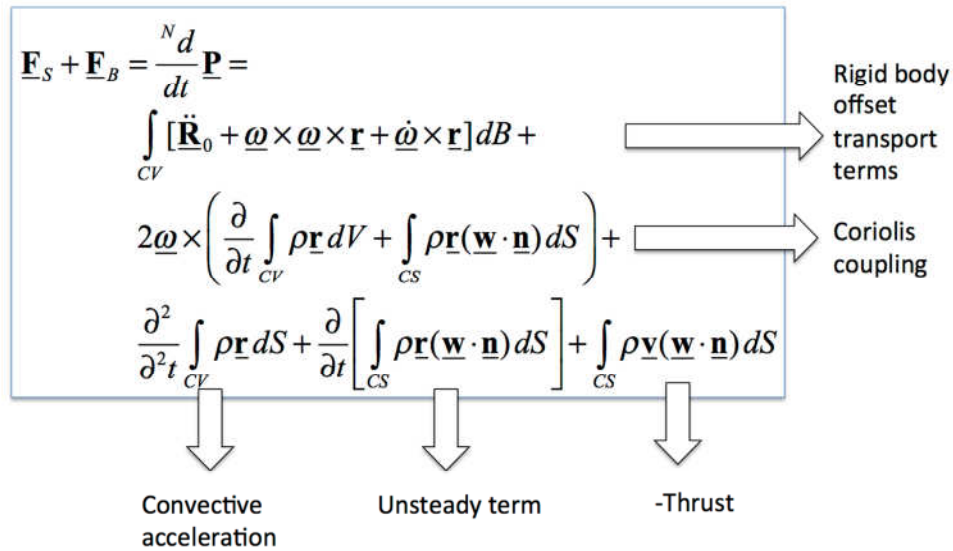
Hence, the angular momentum balance about O' is:

$$\sum \underline{M}_{O'} = \underline{R} \times \left(\underline{F}_B + \underline{F}_S \right) + \frac{\partial \underline{I}_O}{\partial t} \cdot \underline{\omega}$$
$$+ \int_{CV} (\underline{r} \times \underline{a}_o) dm + \underline{I}_O \cdot \underline{\dot{\omega}} + \underline{\omega} \times (\underline{I}_O \cdot \underline{\omega}) + \int_{CS} \rho(\underline{r} \times \underline{\omega} \times \underline{r})(\underline{w}. \underline{dA})$$
$$+ \frac{\partial}{\partial t} \int_{CV} (\underline{r} \times \underline{v}) dm + \int_{CS} \rho(\underline{r} \times \underline{v})(\underline{w}. \underline{dA}) + \underline{\omega} \times \int_{CV} (\underline{r} \times \underline{v}) dm$$

$$(25)$$

Sometimes it is useful to write equations of motion about a fixed point O on the body. For body-fixed point we substitute $\underline{R} = \underline{0}$ in the previous equation:

$$\sum \underline{M}_O = \int_{CV} (\underline{r} \times \underline{a}_o) dm + + \underline{I}_O \cdot \underline{\dot{\omega}} + \underline{\omega} \times (\underline{I}_O \cdot \underline{\omega}) + \frac{\partial \underline{I}_O}{\partial t} \cdot \underline{\omega}$$
$$+ \int_{CS} \rho(\underline{r} \times \underline{\omega} \times \underline{r})(\underline{w}. \underline{dA}) + \int_{CS} \rho(\underline{r} \times \underline{v})(\underline{w}. \underline{dA})$$
$$+ \frac{\partial}{\partial t} \int_{CV} (\underline{r} \times \underline{v}) dm + \underline{\omega} \times \int_{CV} (\underline{r} \times \underline{v}) dm$$

$$(26)$$

Figures 2 and 3 depict the various terms appearing in the linear and the angular momentum balance equations. Notice the appearance of a steady thrust term, an unsteady thrust term, and gyroscopic and Coriolis coupling terms both in the linear and the angular momentum balance.


Figure 2. Summary of Terms in Linear Momentum Balance.

American Institute of Aeronautics and Astronautics

$$\underline{\mathbf{M}}_0 = \frac{{}^N d}{dt} \mathbf{H}_0 =$$

$$= \int\limits_B \mathbf{r} \times \underline{\ddot{\mathbf{R}}}_0 \, dB$$

$$+ \underline{\underline{\mathbf{J}}}_0 \cdot \dot{\underline{\omega}} + \underline{\dot{\underline{\mathbf{J}}}}_0 \cdot \underline{\omega} + \underline{\omega} \times \underline{\underline{\mathbf{J}}}_0 \cdot \underline{\omega}$$

$$+ \int\limits_{CS} \rho \underline{\mathbf{r}} \times (\underline{\omega} \times \mathbf{r})(\underline{\mathbf{w}} \cdot \underline{\mathbf{n}}) \, dS + \underline{\omega} \times \int\limits_{CV} \rho \underline{\mathbf{r}} \times \underline{\mathbf{v}} \, dV$$

$$+ \frac{\partial}{\partial t} \int\limits_{CV} \rho \underline{\mathbf{r}} \times \underline{\mathbf{v}} \, dV + \int\limits_{CS} \rho (\underline{\mathbf{r}} \times \underline{\mathbf{v}})(\underline{\mathbf{w}} \cdot \underline{\mathbf{n}}) \, dS$$

Rigid body offset transport terms

Rigid body Rotational terms

Gyroscopic coupling terms

Unsteady term

-Thrust moment

Figure 3. Summary of Terms in Angular Momentum Balance.

(a) A Double Pendulum

(b) Equivalent Single Pendulum
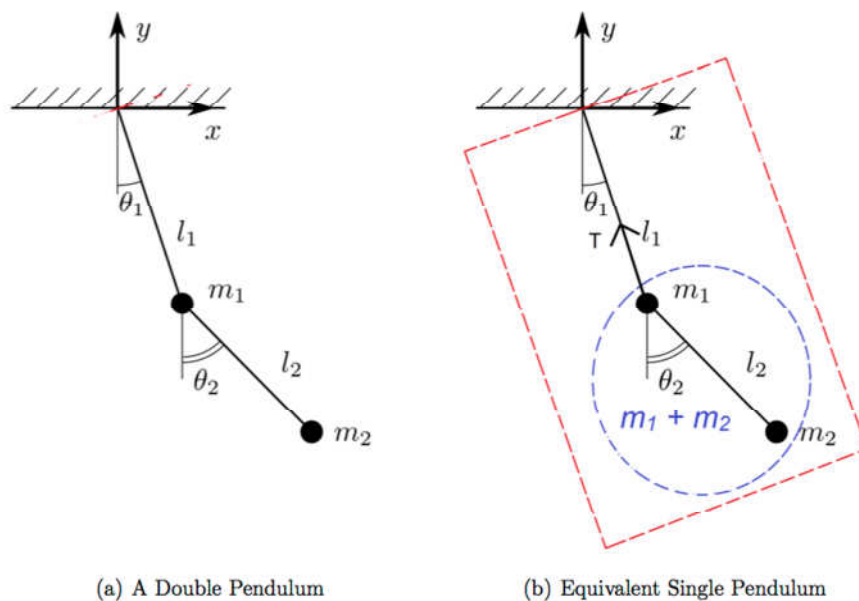
Figure 4. Validation of equations of motion for a double pendulum.

F. Validation for a Double Pendulum System

A double pendulum (see Figure 4.a) is a pendulum with another pendulum attached to its end, and is a simple physical system that exhibits rich dynamic behavior with a strong sensitivity to initial conditions. The motion of a double pendulum is governed by a set of coupled ordinary differential equations given by:

American Institute of Aeronautics and Astronautics

$$(m_1 + m_2)l_1^2\ddot{\theta}_1 + m_2l_1l_2\cos(\theta_2 - \theta_1)\ddot{\theta}_2 - m_2l_1l_2\sin(\theta_2 - \theta_1)\dot{\theta}_2^2 + (m_1 + m_2)gl_1\sin\theta_1 = 0$$
$$m_2l_2^2\ddot{\theta}_2 + m_2l_1l_2\cos(\theta_2 - \theta_1)\ddot{\theta}_1 + m_2l_1l_2\sin(\theta_2 - \theta_1)\dot{\theta}_1^2 +$$
$$m_2gl_2\sin\theta_2 = 0 \qquad (27)$$

However, we look at this double pendulum system in a different way. We treat this complex pendulum system as an equivalent single pendulum with mass $(m_1 + m_2)$ and rotating with the first link (see Figure 4.b). However, because of the movement of the second link, there is a redistribution of mass inside the complex bob of mass $(m_1 + m_2)$, thereby changing the inertia of the system about the hinge O and the location of the COM. Our goal is to obtain the same set of governing equations using the dynamical equations derived in the previous section. For our convenience, we assume that both the inertial frame and the body frame are located at O, with the body frame rotating with the first link. We note that the motion is always planar and there is no mass-flow in or out of the system. Since the motion of the body is planar, we have:

$$\underline{\omega} = \begin{bmatrix} 0 \\ 0 \\ \dot{\theta}_1 \end{bmatrix} \qquad (28)$$

If $\underline{I}_O$ is the inertia tensor of the body about O, we have:

$$\underline{I}_O \cdot \underline{\omega} = \begin{bmatrix} 0 \\ 0 \\ I_{zz}\dot{\theta}_1 \end{bmatrix} \qquad (29)$$

Hence the gyroscopic coupling term becomes:

$$\underline{\omega} \times \left(\underline{I}_O \cdot \underline{\omega}\right) = \underline{0} \qquad (30)$$

The moment of inertia about z-axis is given by:

$$I_{zz} = m_1l_1^2 + m_2(l_1^2 + l_2^2 + 2l_1l_2\cos(\theta_2 - \theta_1)) \qquad (31)$$

$$\Rightarrow \left(\frac{dI_O}{dt}\right) \cdot \underline{\omega} = \begin{bmatrix} 0 \\ 0 \\ -2m_2l_1l_2\sin(\theta_2 - \theta_1)(\dot{\theta}_2 - \dot{\theta}_1)\dot{\theta}_1 \end{bmatrix} \qquad (32)$$

Hence, the Newton-Euler equations for the equivalent single pendulum system are:

$$\sum \underline{M}_O^{ext} = \underline{I}_O \cdot \underline{\alpha} + \left(\frac{dI_O}{dt}\right) \cdot \underline{\omega} + \int_{CV} (\underline{\omega} \times \underline{r} \times \underline{v})dm + \frac{\partial}{\partial t}\int_{CV} (\underline{r} \times \underline{v})dm \qquad (33)$$

$$\sum \underline{F}^{ext} = \int_{CV} \{(\underline{\dot{\omega}} \times \underline{r}) + (\underline{\omega} \times \underline{\omega} \times \underline{r})\}dm + 2\underline{\omega} \times \frac{\partial}{\partial t}\int_{CV} \underline{r}dm + \frac{\partial^2}{\partial t^2}\int_{CV} \underline{r}dm \quad (34)$$

Also, the position vector of the masses from the point O are:

$$\underline{r}_1 = \begin{bmatrix} l_1\sin\theta_1 \\ -l_1\cos\theta_1 \\ 0 \end{bmatrix} \qquad \underline{r}_2 = \begin{bmatrix} l_1\sin\theta_1 + l_2\sin\theta_2 \\ -l_1\cos\theta_1 - l_2\cos\theta_2 \\ 0 \end{bmatrix} \qquad (35)$$

If $\underline{v}_1, \underline{v}_2, \underline{a}_1$ and $\underline{a}_2$ are the velocities and accelerations of the two masses as observed in the body frame (described in the inertial frame), we have:

$$\underline{v}_1 = \underline{0}$$
$$\underline{a}_1 = \underline{0}$$

$$\underline{v}_2 = \begin{bmatrix} l_2 \cos \theta_2 (\dot{\theta}_2 - \dot{\theta}_1) \\ l_2 \sin \theta_2 (\dot{\theta}_2 - \dot{\theta}_1) \\ 0 \end{bmatrix}$$

$$\underline{a}_2 = \begin{bmatrix} l_2 \cos \theta_2 (\dot{\theta}_2 - \dot{\theta}_1) - l_2 \sin \theta_2 (\dot{\theta}_2 - \dot{\theta}_1)^2 \\ l_2 \sin \theta_2 (\dot{\theta}_2 - \dot{\theta}_1) + l_2 \cos \theta_2 (\dot{\theta}_2 - \dot{\theta}_1)^2 \\ 0 \end{bmatrix} \tag{36}$$

Hence, we have:

$$\int_{CV} (\underline{\omega} \times \underline{r} \times \underline{v}) dm = m_2 (\underline{\omega} \times \underline{r_2} \times \underline{v_2}) = \underline{0} \tag{37}$$

$$\frac{\partial}{\partial t} \int_{CV} (\underline{r} \times \underline{v}) dm = m_2 (\underline{r_2} \times \underline{a_2}) = \underline{0} \tag{38}$$

$$2\underline{\omega} \times \frac{\partial}{\partial t} \int_{CV} \underline{r} dm = (2\underline{\omega} \times \underline{v_2}) m_2 \tag{39}$$

$$\frac{\partial^2}{\partial t^2} \int_{CV} \underline{r} dm = m_2 \underline{a}_2 \tag{40}$$

The net external moment about point O is:

$$\sum \underline{M}_O^{ext} = \begin{bmatrix} 0 \\ 0 \\ -m_1 g l_1 \sin \theta_1 - m_2 g (l_1 \sin\theta_1 + l_2 \sin\theta_2) \end{bmatrix} \tag{41}$$

Substituting above terms into the Euler's equation for the equivalent single pendulum system, we obtain:

$$(m_1 + m_2) l_1^2 \ddot{\theta}_1 + m_2 l_2^2 \ddot{\theta}_2 + m_2 l_1 l_2 \cos(\theta_2 - \theta_1)(\ddot{\theta}_1 + \ddot{\theta}_2)$$
$$+ m_2 l_1 l_2 \sin(\theta_2 - \theta_1)(\dot{\theta}_1^2 - \dot{\theta}_2^2) + (m_1 + m_2) g l_1 \sin \theta_1 + m_2 g \, l_2 \sin \theta_2 = 0$$

$$\tag{42}$$

Similarly, net external force on the mass $(m_1 + m_2)$ is:

$$\sum \underline{F}^{ext} = \begin{bmatrix} -T \sin \theta_1 \\ T \cos \theta_1 - (m_1 + m_2) g \\ 0 \end{bmatrix} \tag{43}$$

where, T is the Tension force acting on the pendulum bob. Substituting above terms into the linear momentum balance for the equivalent single pendulum system, we obtain:

$$(m_1 + m_2) l_1 \cos \theta_1 \, \ddot{\theta}_1 + m_2 l_2 \cos \theta_2 \, \ddot{\theta}_2 -$$
$$(m_1 + m_2) l_1 \sin \theta_1 \, \dot{\theta}_1^2 - m_2 l_2 \sin \theta_2 \dot{\theta}_2^2 = -T \sin \theta_1$$

$$(m_1 + m_2) l_1 \sin \theta_1 \, \ddot{\theta}_1 + m_2 l_2 \sin \theta_2 \, \ddot{\theta}_2 +$$
$$(m_1 + m_2) l_1 \cos \theta_1 \, \dot{\theta}_1^2 - m_2 l_2 \cos \theta_2 \, \dot{\theta}_2^2 = T \cos \theta_1 - (m_1 + m_2) g$$

$$\tag{44}$$

Multiplying equation (42a) by $(l_1 \cos \theta_1)$ and equation (42b) by $(l_1 \sin \theta_1)$ and adding the two equations, we obtain:

$$(m_1 + m_2)l_1^2 \ddot{\theta}_1 + m_2 l_1 l_2 \cos(\theta_2 - \theta_1)\,\ddot{\theta}_2 - m_2 l_1 l_2 \sin(\theta_2 - \theta_1)\dot{\theta}_2^2$$
$$+ (m_1 + m_2)gl_1 \sin \theta_1 = 0$$

(45)

Subtracting equation 43 from equation 40, we obtain:

$$m_2 l_1 l_2 \cos(\theta_2 - \theta_1)\,\ddot{\theta}_1 + m_2 l_2^2 \ddot{\theta}_2 + m_2 l_1 l_2 \sin(\theta_2 - \theta_1)\dot{\theta}_1^2 + m_2 gl_2 \sin \theta_2 = 0$$

(46)

Thus, we observe that the two equations 43, 44 obtained using Transport Theorem are indeed the governing equations of motion for a double pendulum system.

G. Comparison to Previously Established Work (Thomson[10])

Thomson described equations of motion for variable mass systems by analyzing the motion of a system of point masses. This section of the article deals with re-deriving the Newton's equation by using the Transport Theorem approach as described earlier. In order to be consistent with the notations used by Thomson, we describe the following notations:

$$\underline{\rho}_{oi} : \text{position of i}^{\text{th}} \text{ particle in the rotating frame}$$
$$\underline{\dot{\rho}}_{oi_{rel}} : \text{velocity of i}^{\text{th}} \text{ particle in the rotating frame}$$
$$\underline{\rho}_{oc} : \text{position of COM in the rotating frame}$$
$$\underline{\dot{\rho}}_{oc_{rel}} : \text{velocity of COM in the rotating frame}$$
$$\underline{r}_i : \text{position of i}^{\text{th}} \text{ particle in the fixed frame}$$
$$\underline{r}_c : \text{position of COM in the fixed frame}$$
$$\iint \rho\left(\underline{w}.\underline{dA}\right) = -\dot{m}$$

Hence, the linear momentum balance for this system can be re-written as:

$$\underline{F}_B + \underline{F}_S = \sum_B m_i \left\{ \underline{a}_o + \underline{\dot{\omega}} \times \underline{\rho}_{oi} + \underline{\omega} \times \left(\underline{\omega} \times \underline{\rho}_{oi} \right) \right\}$$
$$+ 2\underline{\omega} \times \left(\frac{\partial}{\partial t} \sum_B m_i \, \underline{\rho}_{oi} \right) - 2\underline{\omega} \times \dot{m}\underline{\rho}_{oe}$$
$$+ \frac{\partial^2}{\partial t^2} \sum_B m_i \, \underline{\rho}_{oi} - \frac{\partial \left(\dot{m}\underline{\rho}_{oe} \right)}{\partial t} - \dot{m}\underline{u} \qquad (47)$$

Now, by definition of COM,

$$\sum_B m_i \, \underline{\rho}_{oi} = m\underline{\rho}_{oc} \qquad (48)$$

$$\Rightarrow \frac{\partial}{\partial t} \sum_B m_i \, \underline{\rho}_{oi} = \dot{m}\underline{\rho}_{oc} + m\underline{\dot{\rho}}_{oc_{rel}} \qquad (49)$$

$$\Rightarrow \frac{\partial^2}{\partial t^2} \sum_B m_i \, \underline{\rho}_{oi} = \ddot{m}\underline{\rho}_{oc} + m\underline{\ddot{\rho}}_{oc_{rel}} + 2\dot{m}\underline{\dot{\rho}}_{oc_{rel}} \qquad (50)$$

$$\Rightarrow \frac{\partial \left(\dot{m}\underline{\rho}_{oe} \right)}{\partial t} = \ddot{m}\underline{\rho}_{oe} \tag{51}$$

Hence, the baance of forces can be re-written as:

$$\underline{F}_B + \underline{F}_S = m\underline{a}_O + m\underline{\dot{\omega}} \times \underline{\rho}_{oc} + m\left(\underline{\omega} \times \left(\underline{\omega} \times \underline{\rho}_{oc} \right) \right)$$
$$+ 2\underline{\omega} \times \dot{m}\left(\underline{\rho}_{oc} - \underline{\rho}_{oe} \right) + 2\underline{\omega} \times m\underline{\dot{\rho}}_{oc_{rel}}$$
$$+ \ddot{m}\left(\underline{\rho}_{oc} - \underline{\rho}_{oe} \right) + m\underline{\ddot{\rho}}_{oc_{rel}} + \dot{m}\left(2\underline{\dot{\rho}}_{oc_{rel}} - \underline{u} \right) \tag{52}$$

However, from kinematics we know:

$$\underline{\ddot{r}}_C = \underline{a}_O + \left(\underline{\dot{\omega}} \times \underline{\rho}_{oc} \right) + \underline{\omega} \times \left(\underline{\omega} \times \underline{\rho}_{oc} \right) + 2\underline{\omega} \times \underline{\dot{\rho}}_{oc_{rel}} + \underline{\ddot{\rho}}_{oc_{rel}}$$
$$\Rightarrow \underline{F} = m\underline{\ddot{r}}_C - \dot{m}\left[2\underline{\omega} \times \left(\underline{\rho}_{oe} - \underline{\rho}_{oc} \right) - 2\underline{\dot{\rho}}_{oc_{rel}} + \underline{u} \right] - m\left(\underline{\ddot{\rho}}_{oe} - \underline{\ddot{\rho}}_{oc} \right) \tag{53}$$

As observed, the above equation has the exact same form as derived in Thomson's paper.

H. Comparison to Previously Established Work (Cornelisse[3])

Cornelisse et al. derived the equations of motion of a rigid rocket. If the origin of the body frame is located at the COM, the linear momentum balance equation can be re-written as:

$$\underline{F}_B + \underline{F}_S = \int_{CV} \rho \left\{ \underline{a}_O + \underbrace{\underline{\dot{\omega}} \times \underline{r}}_{=0} + \underbrace{\underline{\omega} \times \left(\underline{\omega} \times \underline{r} \right)}_{=0} \right\} d\forall$$

$$+ 2\underline{\omega} \times \underbrace{\left(\frac{\partial}{\partial t} \underbrace{\int_{CV} \rho\underline{r}\, d\forall}_{=0} + \int_{CS} \rho\underline{r}\left(\underline{w}.\underline{dA} \right) \right)}_{-\underline{F}_C, Coriolis\ Force}$$

$$+ \underbrace{\frac{\partial^2}{\partial t^2} \underbrace{\int_{CV} \rho\underline{r}\, d\forall}_{=0} + \frac{\partial}{\partial t} \int_{CS} \rho\underline{r}\left(\underline{w}.\underline{dA} \right) + \int_{CS} \rho\underline{v}\left(\underline{w}.\underline{dA} \right)}_{-\underline{F}_{rel}, Transport\ Theorem\ in\ Rotating\ Frame}$$

$$\tag{54}$$

Or equivalently,

$$\underline{F}_B + \underline{F}_S + \underline{F}_C + \underline{F}_{rel} = m\frac{d'\underline{v}_{cm}}{d't} \tag{55}$$

where, $\underline{F}_C = 2\underline{\omega} \times \dot{m}\underline{r}_e$ and $\underline{F}_{rel} = \frac{\partial(\dot{m}\underline{r}_e)}{\partial t} + \dot{m}\underline{U}_{rel}$. The Coriolis Force, $\underline{F}_C$ term matches the one in Cornelisse (4.2-6). The Relative Force, $\underline{F}_{rel}$ term matches the one in Cornelisse (4.2-12). The final equation 55 has the same form as 4.2-1 in Cornelisse. Similarly, the angular momentum balance equation for a rigid rocket has the same form as described in Cornelisse.

Figure 5. Flight profile of SIAD test.

$$ECI \quad \rightarrow \quad R_3(\omega_E t) \rightarrow \quad ECEF$$

$$ECEF \quad \rightarrow R_2(180^o)R_2(90^o - lat)R_3(long) \rightarrow NED$$

$$NED \quad \rightarrow \quad R_3(yaw)R_2(pitch)R_1(roll) \quad \rightarrow \quad B$$
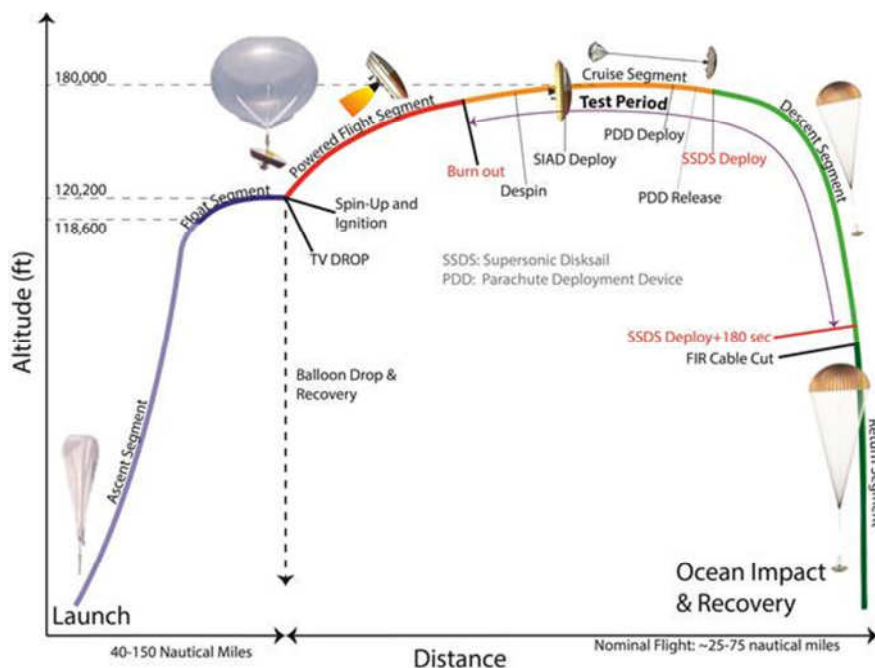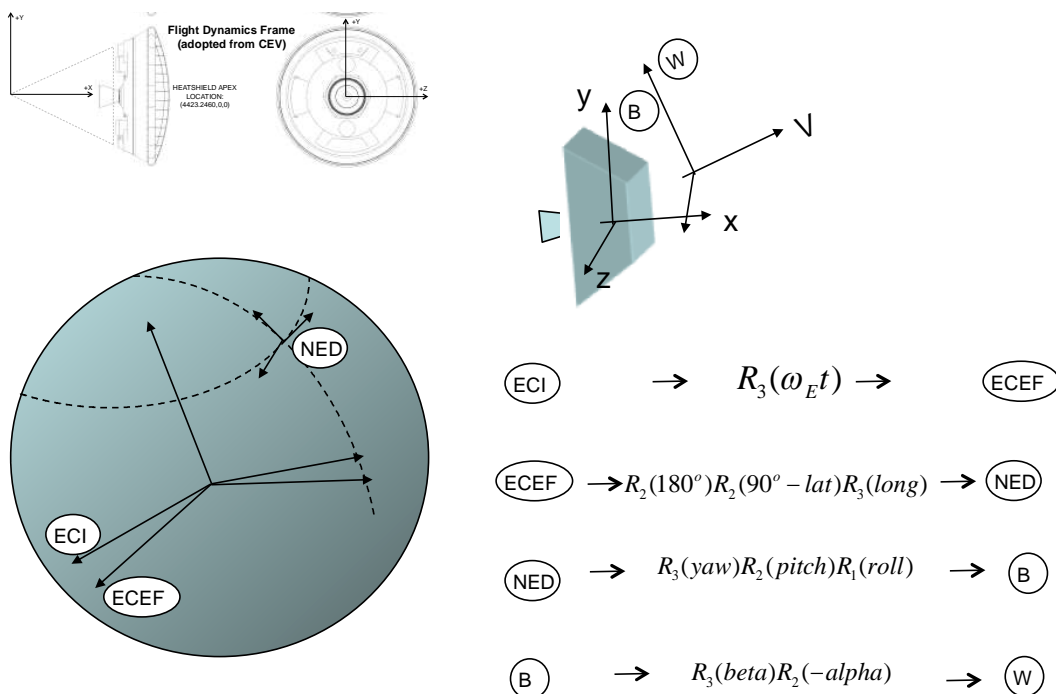
$$B \quad \rightarrow \quad R_3(beta)R_2(-alpha) \quad \rightarrow \quad W$$

Figure 6. Frames and transformations used.

III.   Equations of Motion of Variable Mass Spinning System under Thrust

Future robotic missions to Mars and eventual human exploration of the Red Planet will require that more massive payloads than the one-ton Curiosity Mars rover be delivered to the surface[9]. NASA is developing new large, sturdy,

American Institute of Aeronautics and Astronautics

and lightweight systems to deliver next- generation rovers and landers on Mars. These new technologies would be able to slow larger, heavier landers from the supersonic speeds of Mars atmospheric entry to the subsonic ground-approach speeds necessary for a safe landing. These systems, called low density supersonic decelerators, aim to solve the complicated problem of slowing Martian entry vehicles down enough to safely deliver large payloads to the Martian surface without bringing along massive amounts of extra rocket propellant or carrying a large and heavy atmospheric entry shield. Of Entry, Descent, and Landing (EDL) technology developments over recent years, progress has been made in Entry (e.g. guidance) and Landing (e.g. skycrane concept for the Mars Science Laboratory) but little progress made on Descent (drag devices). NASA is interested in maturing supersonic drag device technology for future robotic and manned missions to Mars. The LDSD (Low Density Supersonic Decelerator) Project[9] was established to fully test two types of drag devices: a) Supersonic Inflatable Aerodynamic Decelerator (SIAD), and b) Supersonic Ringsail Parachute (SRP). During motor burn, a spin rate is used to mitigate the impact of thrust-to-center of mass offset uncertainty on the trajectory flight path during main engine operation, since there is no active control system. A predictable pitch over early in flight as the vehicle trims along the relative velocity vector is critical for targeting the point at the end of the trajectory when the decelerator is inflated. Shortly after main engine cutoff, the vehicle is spun down and the SIAD is deployed. While SIAD is deployed, a minimal residual roll spin rate is desired to avoid masking flight dynamic behavior. Stratospheric tests of the LDSD would conducted in 2014 and 2015 at the Pacific Missile Range Facility operated by the U.S. Navy on Kauai, Hawaii. A large scientific balloon provided by NASA Wallops Flight Facility and the Columbia Scientific Balloon Facility would lift a solid-rocket powered test vehicle to an altitude of about 120,000 feet (37 kilometers). Within the stratosphere, the LDSD payload would undergo a rocket-powered trajectory to reach supersonic speeds and then test the deployment and function of the inflatable decelerators, followed by recovery of the balloon and test vehicle in the ocean.

Figure 5 shows the fight profile of the SIAD test. The mission design elements include: a) a balloon launch; b) a Star48 engine / CEV type configuration; c) the vehicle is spin-stabilized during powered phase; d) the vehicle is aero-stabilized after powered phase; e) the SIAD is deployed at ~Mach 3.75; f) the parachute is deployed at ~Mach 2; and g) the system finally descends on the parachute to a water landing.

Figure 6 depicts the various reference frames used in the analysis: ECI stands for Earth Centered Inertial, ECEF is the Earth Centered Earth Fixed frame (related to the ECI through the Earth's spin rate), NED is the North-East-Down frame (related to the ECEF frame through the local latitude and longitude), B is the vehicle's body frame (related to the NED through the vehicle's roll, pitch and yaw angles), and W is the aerodynamic wind frame, related to the B frame through the angle-of-attack and sideslip angles.

The equations of motion of the SIAD decelerator as a variable mass spinning system under thrust are derived from following assumptions: a) Spherical Earth rotating at constant rate of rotation of ECEF frame wrt. ECI frame; b) Trajectory wrt. ECEF parameterized via magnitude of radius vector, geodetic latitude, longitude; c) U.S. standard atmosphere model; d) Spherical gravity model with J2 and J3; e) Vehicle is a rigid body with varying mass properties; f) Mass properties and their time rates of change updated at every time step; g) Vehicle translation kinematics parameterized via components of position vector of c.o.m. wrt. ECI; h) Vehicle rotation kinematics of B-frame wrt. ECI frame parameterized by quaternion parameters; i) Vehicle rotation kinematics of NED-frame wrt. ECEF-frame parameterized by latitude and longitude angles; j) Vehicle rotation kinematics of B-frame wrt. NED-frame parameterized by roll-pitch-yaw Euler angles; k) Vehicle rotation kinematics of W-frame wrt. B-frame parameterized by alpha and beta angles; l) Thrust applied with no misalignments along spin axis; Spin axis is roll axis; m) Variable mass effects, including jet damping forces and torques, are included; and n) the system dynamics propagation scheme used is a Runge-Kutta integration scheme at 100 Hz, with the output sampled at 1 Hz.

Several assumptions are also made in regards to the gas-dynamic interaction during the propulsive phase. First of all, there are disturbance forces and torques induced on the vehicle by the solid rocket burn. These interaction effects are both steady and unsteady. The steady interaction effects go under the name of Jet Damping. The jet damping produces a stabilizing or destabilizing moment on a spinning vehicle induced by the interaction between the Coriolis forces and pressure field inside combustion chamber due to the steady gas flow. The main assumptions used in the modeling of the steady gas-dynami interaction effects are the following: a) Rocket and combustion gas collectively are an isolated system; b) Solid portion of system is rigid; c) Burning grain surface and nozzle exit are where mass flow occurs; d) Steady angular rates; e) Rocket motion does not affect internal flow; f) System is axisymmetric wrt.

14
American Institute of Aeronautics and Astronautics

the longitudinal axis; g) Fluid flow within control volume is steady and symmetrical about longitudinal axis; h) Fluid particles have no whirling motion relative to the solid portion; and i) gas exit velocity is uniform. The main assumptions used in the modeling of the unsteady gas-dynamic interaction effects are the following: a) Requires high-fidelity modeling of inertial waves inside combustion chamber; b) Jet damping theory applies only to slender rockets. In large spinning motors, there are strong resonant, wavelike interactions between the flow of gases in the motor and the angular motion of the wobbling spacecraft and large nutation growth may then occur. These assumptions are also reviewed in[11]. As a result of these assumptions, some terms in the linear and angular momentum balance can be dropped out. These simplifications are summarized in Figures 7 and 8.

Figure 7. Thrust dependent terms in linear momentum balance.

Figure 8. Thrust dependent terms in angular momentum balance.

Figure 9 shows the mass and mass flow rate as a function of time during burn. Figure 10 shows the moments of inertia and the rate of change of the moments of inertia during burn, and Figure 11 shows the location of the vehicle's center of mass and applied thrust, as a function of time.
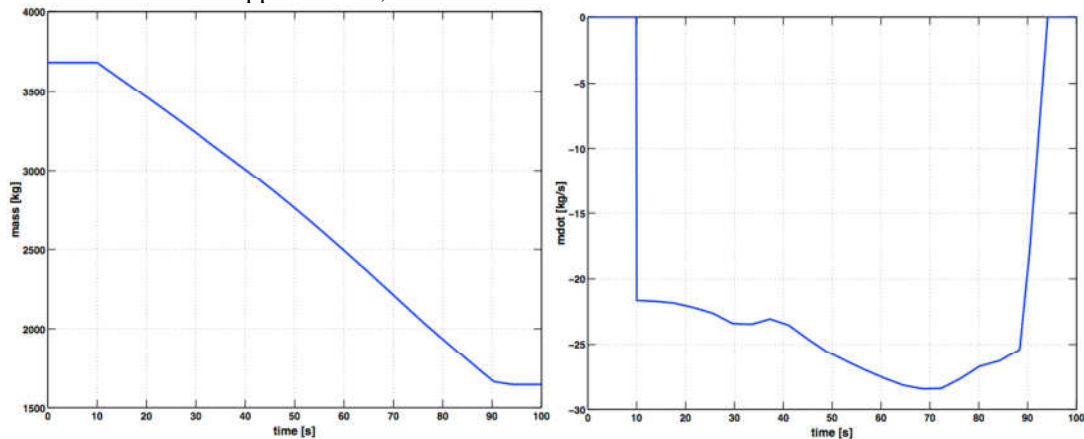
Figure 9. Mass and mass rate of change as a function of time.

16
American Institute of Aeronautics and Astronautics
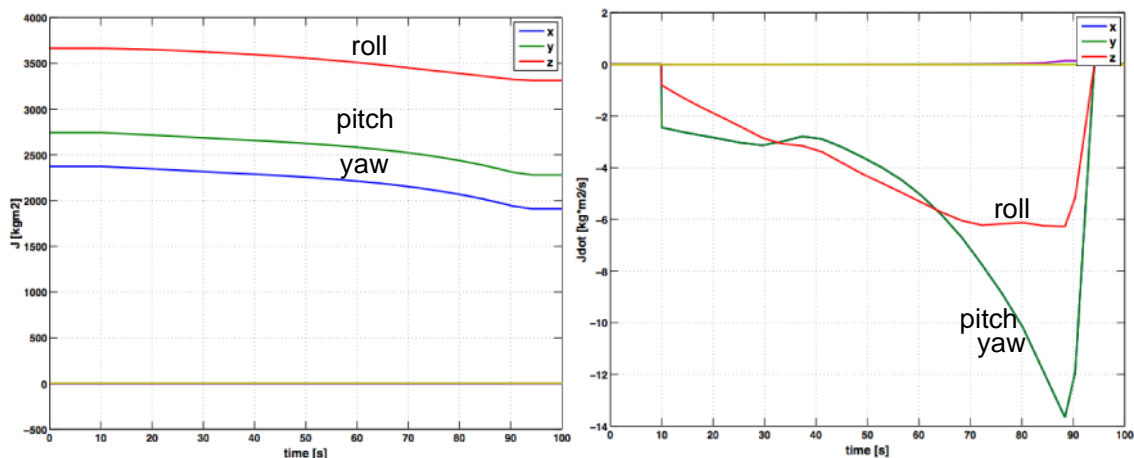
Figure 10. Moments of inertia and their rate of change as a function of time.
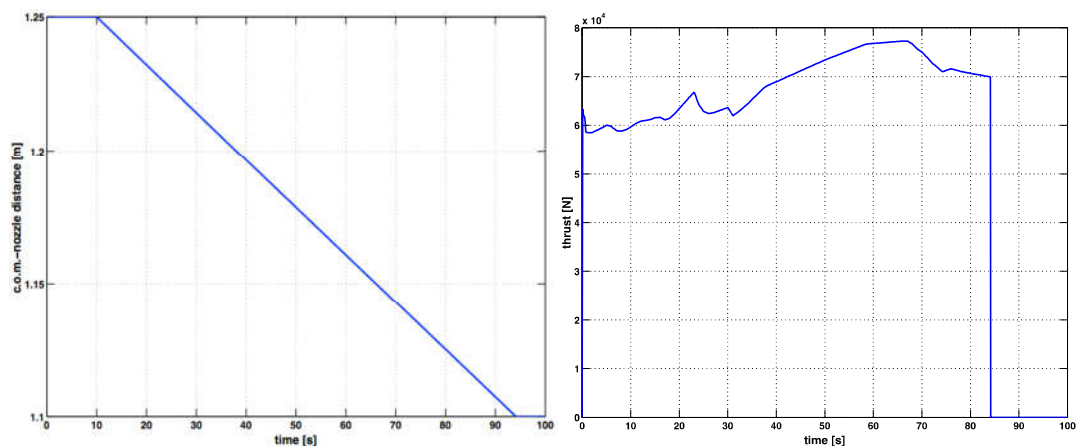

Figure 11. Location of the center of mass and applied thrust, as a function of time.

I. Steady Gas-Dynamic Effects

With the simplifications shown in Figures 8 and 9, the linear momentum balance equation becomes:

American Institute of Aeronautics and Astronautics

$$m\left[\mathbf{a}_0 + \alpha \times \mathbf{r} + \omega \times (\omega \times \mathbf{r})\right] =$$
$$\mathbf{F}_{ext}$$
$$-2\omega \times \int_{S_0} \rho \mathbf{r}(\mathbf{v}_r \cdot \mathbf{n})dS$$
$$-\int_{S_0} \rho \mathbf{v}_r(\mathbf{v}_r \cdot \mathbf{n})dS$$
$$-\frac{{}^B d}{dt}\int_{V_0} \rho \mathbf{v}_r dV$$
$$-2\omega \times \frac{{}^B d}{dt}\int_{V_0} \rho \mathbf{r} dV \tag{56}$$

and the angular momentum balance equations become:

$$\mathbf{I}\dot{\omega} + \omega \times \mathbf{I}\omega = \mathbf{M}_{ext}$$
$$+\rho_e \times \mathbf{T}$$
$$-\dot{\mathbf{I}}\omega$$
$$-\int_{S_c}\left[\mathbf{p} \times (\omega \times \mathbf{p})\right](\rho \mathbf{v}_r \cdot \mathbf{n})dS$$
$$-\int_{V_c} \rho\left[\omega \times (\mathbf{p} \times \mathbf{v}_r)\right]dV$$
$$-\frac{{}^B d}{dt}\int_{V_c} \rho(\mathbf{p} \times \mathbf{v}_r)dV$$
$$-\int_{S_c} \rho(\mathbf{p} \times \mathbf{v}_r)(\mathbf{v}_r \cdot \mathbf{n})dS \tag{57}$$

Here, we have used the following definition for the mass flow rate:

$$\dot{m}_c = -\int_{S_c} \rho(\mathbf{v}_r \cdot \mathbf{n})dS \tag{58}$$

Following Cornelisse, and introducing the equivalent "mass flow center vector", i.e., the location in body frame of the thrust resultant over the nozzle area:

$$\rho_e = \frac{1}{\dot{m}_c}\int_{S_0} \rho \mathbf{r}(\mathbf{v}_r \cdot \mathbf{n})dS \tag{59}$$

the "apparent forces and moments" due to the steady gas dynamic effects can be written as:

$$\mathbf{F}_{app} = -2\omega \times \int_{S_0} \rho \mathbf{r}\left(\mathbf{v}_r \cdot \mathbf{n}\right)dS$$

$$-\int_{S_0} \rho \mathbf{v}_r\left(\mathbf{v}_r \cdot \mathbf{n}\right)dS$$

$$-\frac{^B d}{dt}\int_{V_0} \rho \mathbf{v}_r dV \qquad (60)$$

$$-2\omega \times \frac{^B d}{dt}\int_{V_0} \rho \mathbf{r}dV$$

$$\Rightarrow 2\dot{m}_c \omega \times \rho_e + \mathbf{T}$$

$$\mathbf{M}_{app} = -\int_{S_c}\left[\mathbf{p}\times\left(\omega \times \mathbf{p}\right)\right]\left(\rho \mathbf{v}_r \cdot \mathbf{n}\right)dS$$

$$-\int_{V_c} \rho\left[\omega \times\left(\mathbf{p}\times \mathbf{v}_r\right)\right]dV$$

$$-\frac{^B d}{dt}\int_{V_c} \rho\left(\mathbf{p}\times \mathbf{v}_r\right)dV$$

$$-\int_{S_c} \rho\left(\mathbf{p}\times \mathbf{v}_r\right)\left(\mathbf{v}_r \cdot \mathbf{n}\right)dS \qquad (61)$$

$$\Rightarrow \dot{m}_c \rho_e \times \omega \times \rho_e + \rho_e \times \mathbf{T}$$

As shown in Figures 8 and 9, other terms vanish on account of: a) the solid portion of system is rigid; b) System is axisymmetric wrt. longitudinal axis; c) Fluid flow within control volume is steady and symmetrical about longitudinal axis; and d) Fluid particles have no whirling motion relative to the solid portion of the system. Therefore, the final equations of motion, used for simulation of the system during the propulsive phase, are:

$$\dot{\mathbf{r}} = \mathbf{v}$$

$$\dot{\mathbf{q}} = \frac{1}{2}\left[\begin{array}{c}\tilde{\mathbf{q}}_v\omega + q_s\omega \\ -\mathbf{q}_v^T\end{array}\right] \qquad (62)$$

for the kinematics, and

$$m\left[\mathbf{a}_0 + \alpha \times \mathbf{r} + \omega \times\left(\omega \times \mathbf{r}\right)\right] = \mathbf{F}_{ext} + 2\dot{m}_c \omega \times \rho_e + \mathbf{T}$$

$$\mathbf{I}\dot{\omega} + \omega \times \mathbf{I}\omega = \mathbf{M}_{ext} - \dot{\mathbf{I}}\omega + \dot{m}_c \rho_e \times \omega \times \rho_e + \rho_e \times \mathbf{T} \qquad (63)$$

for the linear and angular momentum balance. Notice the Coriolis-like terms due to mass flow in the translation dynamics, the "jet-damping" terms and the moment due to the thrust (thrust misalignment moment) in the rotational equations. These equations are consistent with those derived in Cornelisse and Eke.

J. Considerations on System Stability

If we observe the homogeneous rotational equations in (63), and use (p,q,r) for the roll, pitch and yaw rates, assuming no external forces, and no thrust misalignment moment, we obtain:

$$I_s\dot{p} + \left(\dot{I}_s - c_1\dot{m}R_n^2\right)p = 0$$

$$I_t\dot{q} - (I_t - I_s)qr + \left(\dot{I}_t - c_2\dot{m}\rho_e^2\right)q = 0$$

$$I_t\dot{r} + (I_t - I_s)qr + \left(\dot{I}_t - c_2\dot{m}\rho_e^2\right)r = 0$$

(64)

We can assume a harmonic approximation for the solution of these equations, and we can obtain the following homogeneous solutions:

$$p(t) = p(0)e^{\left\{-\int_0^t\left[\left(\dot{I}_s - c_1\dot{m}R_n^2\right)/I_s\right]dt\right\}}$$

(65)

$$q(t) + ir(t) = \left[q(0) + ir(0)\right]e^{\left\{-\int_0^t\left[\left(\dot{I}_t - c_2\dot{m}\rho_e^2\right)/I_t\right]dt\right\}}e^{i\int_0^t\left[(I_t - I_s)/I_t\right]dt}$$

from which we note that the system dynamics is stable if the following conditions are satisfied:

$$\left(\dot{I}_s - c_1\dot{m}R_n^2\right) < 0$$

$$\int_0^t\left[\left(\dot{I}_t - c_2\dot{m}\rho_e^2\right)/I_t\right]dt > 0$$

(66)

Figure 12 shows the vehicle roll time constant as a function of time, indicating that, for the variable mass parameters assumed for this vehicle (shown in Figures 9, 10, and 11), the roll channel is unstable and, given an initial roll rate, the vehicle is expected to accelerate under thrust. Conversely, the combined pitch and yaw channels are stable, and theis initial rate should decay to zero during thrust. The simulation results, described later on, will confirm these assessments.
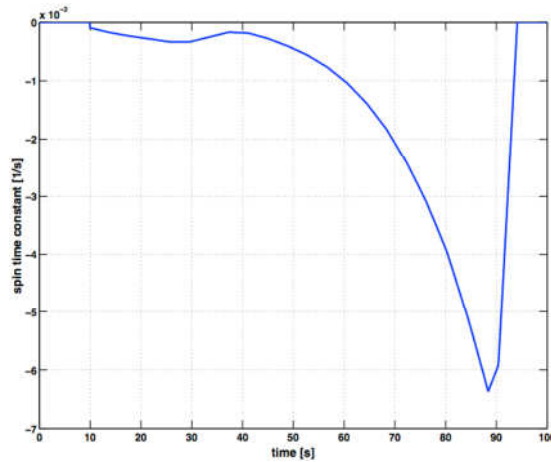
Figure 12. Roll time constant as a function of time.

K. Uniform and Non-Uniform Exit Flow

The equations of motion (equation 63) have been specialized for various profiles of exit velocity distribution. This development follows the work by Eke et al[4,5,6,12]. In Eke, the angular momentum balance

20
American Institute of Aeronautics and Astronautics

is rewritten as:

$$\mathbf{I}\dot{\omega} + \omega \times \mathbf{I}\omega = -\dot{\mathbf{I}}\omega - \int_{S_c}\left[\mathbf{p}\times(\omega\times\mathbf{p})\right](\rho\mathbf{v}_r\cdot\mathbf{n})dS$$

(67)

where the point of thrust application p, and the mass flow rates, for uniform exit velocity, become:

$$\mathbf{p} = x_e\mathbf{b}_1 + r\cos\theta\mathbf{b}_2 + r\sin\theta\mathbf{b}_3$$

(68)

$$\mathbf{v}_r\cdot\mathbf{n} = u = \text{constant}$$

(69)

$$\dot{m}_c = -\int_{S_c}\rho(\mathbf{v}_r\cdot\mathbf{n})dS = -\pi x_e u R_n^2$$

(70)

$$\rho_e = \left(\begin{array}{ccc} \rho_e & \dfrac{R_n}{2} & \dfrac{R_n}{2} \end{array}\right)$$

(71)

The mass flow term in equation (67) becomes:

$$\int_{S_c}\left[\mathbf{p}\times(\omega\times\mathbf{p})\right](\rho\mathbf{v}_r\cdot\mathbf{n})dS = -\dot{m}_c\left[\frac{R_n^2}{2}\omega_x\mathbf{b}_1 + \left(x_e^2 + \frac{R_n^2}{4}\right)(\omega_y\mathbf{b}_2 + \omega_z\mathbf{b}_3)\right]$$

(72)

And, consistently with Eke, the final rotational equations are:

$$I_1\dot{\omega}_1 + (I_3 - I_2)\omega_2\omega_3 + [\dot{I}_1 - \dot{m}(\rho_e^2 + \frac{R_n^2}{4})]\omega_1 = M_1$$

$$I_2\dot{\omega}_2 + (I_1 - I_3)\omega_3\omega_1 + [\dot{I}_2 - \dot{m}(\rho_e^2 + \frac{R_n^2}{4})]\omega_2 = M_2$$

$$I_3\dot{\omega}_3 + (I_2 - I_1)\omega_1\omega_2 + [\dot{I}_3 - \dot{m}\frac{R_n^2}{2}]\omega_3 = M_3$$

(73)

If the exit velocity is non-uniform, the rotational equations become:

$$\mathbf{I}\dot{\omega} + \omega\times\mathbf{I}\omega = \mathbf{M}_{ext} - \dot{\mathbf{I}}\omega + \rho_e\times\mathbf{T} - \int_{S_c}\left[\mathbf{p}\times(\omega\times\mathbf{p})\right](\rho\mathbf{v}_r\cdot\mathbf{n})dS$$

$$\mathbf{v}_r\cdot\mathbf{n} = u(r)$$

(74)

and, defining the following f and g parameters, function of the exit nozzle radius R_n:

American Institute of Aeronautics and Astronautics

$$f = \rho_e^2 + \frac{R_n^2}{4}, \quad g = \frac{R_n^2}{2} \text{ (uniform)}$$

$$f = \rho_e^2 + \frac{3R_n^2}{20}, \quad g = \frac{3R_n^2}{10} \text{ (linear)} \tag{75}$$

$$f = \rho_e^2 + \frac{R_n^2}{6}, \quad g = \frac{R_n^2}{3} \text{ (parabolic)}$$

the final rotational equations for the case of non-uniform exit velocity become:

$$I_1\dot{\omega}_1 + (I_3 - I_2)\omega_2\omega_3 + [\dot{I}_1 - \dot{m}f]\omega_1 = M_1$$
$$I_2\dot{\omega}_2 + (I_1 - I_3)\omega_3\omega_1 + [\dot{I}_2 - \dot{m}f]\omega_2 = M_2$$
$$I_3\dot{\omega}_3 + (I_2 - I_1)\omega_1\omega_2 + [\dot{I}_3 - \dot{m}g]\omega_3 = M_3$$

$$(76)$$

Figure 13 shows the forces and torques arising from the steady gas-dynamic interaction, i.e. the "jet-damping" terms. Figure 14 (left) shows the spin rate during the burn for uniform, linear and parabolic gas exit velocity profiles, indicating a growth in the spin rate. Figure 14 (right) shows the spin rate for different values of the exit nozzle radius, indicating that when the nozzle radius is large, the effective result on the spin rate is to decrease it, instead of increasing it. This result is consistent with the results observed in 1975 during the propulsive tests for the Viking vehicle[2]. The BLDT vehicle had four large retrorockets, canted with respect to the longitudinal axis, effectively forming a large effective exit radius, and the test results indicated that at the end of the test the vehicle had slowed own its roll body rate. The SIAD vehicle, instead, ha only one rocket along the longitudinal axis and, effectively, a much smaller exit radius that the BLDT.
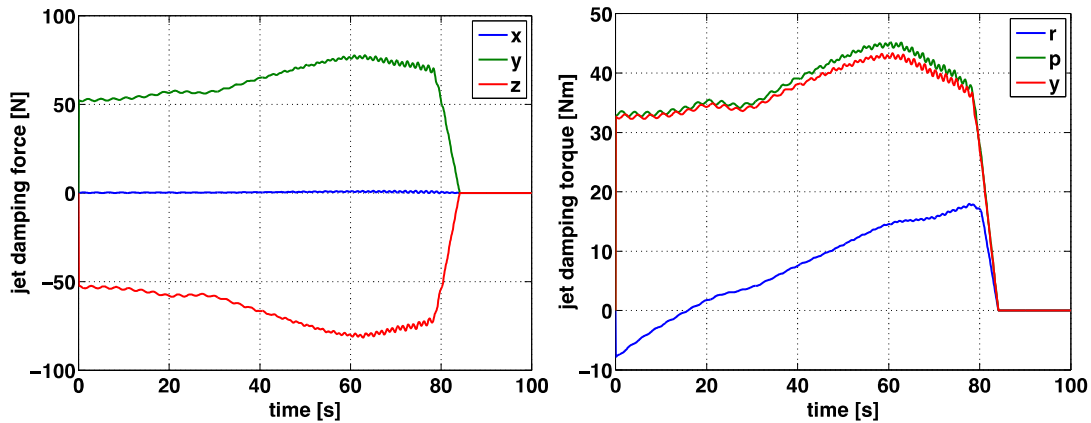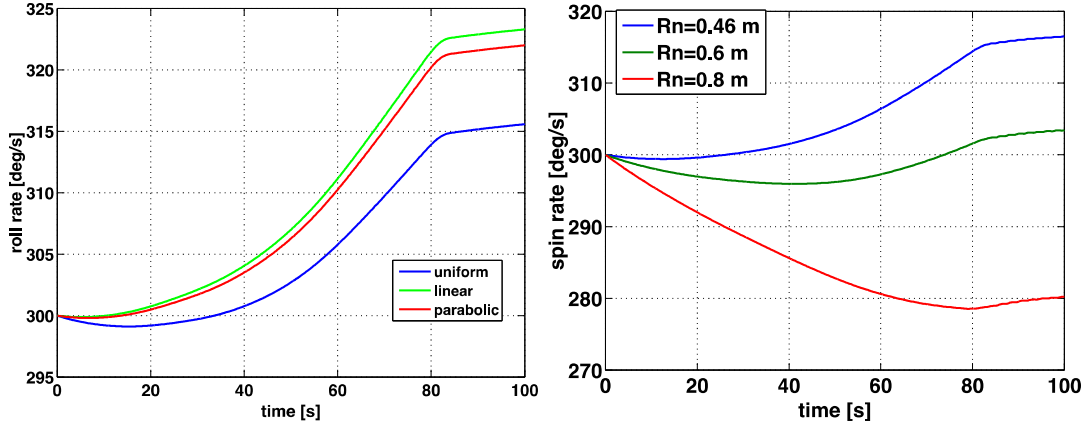

Figure 13. Jet damping forces and torques, during burn.

Figure 14. Roll (spin) rate during burn, as a function of exit velocity profile (left) and exit radius (right).

L. Unsteady Gas-Dynamic Effects

STAR-48 motors are prone to coning instability (nutation amplification due to unfavorable gas-dynamic interactions) which has been observed on several occasions[11]. The observed STAR-48 burn dynamics for past prolate payloads indicated that:

- at t=0 sec: Start of burn. Dominated by small residual wobble induced during spin---up. Rates usually less than 1 deg/sec.
- at t=50 sec: Mid-burn. Short periods of coning growth/decay followed by sustained growth during last 10 seconds of motor burn.
- at t=87 sec: End of motor burn. Lateral angular rates may exceed 15 to 60 deg/s. Final cone angle is in the range 5-20 deg depending on initial wobble angle, vehicle moments of inertia, and spin rate.

The STAR-48B (Long Nozzle) motor was successfully used as an upper stage of the Delta II launch vehicle on over 90 missions from 1989-2009. All flights were exo-atmospheric (SIAD flight is endo-atmospheric). A comparison of key flight dynamics parameters previously done by industry indicated that LDSD was outside of Delta II flight experience for several key parameters which may limit applicability of empirical data. The Delta II Star-48B flight experience (for prolate payloads) also indicates that the spin-up effect due to jet damping cannot be conclusively predicted based on prior experience.

To fully address this issue, the variable-mass rigid body model described above was extended to account for the internal unsteady gas-dynamic interaction by including modeling of the inertial waves. This derivation follows Ref. 7, and is based on including a corrective term in the rotational equaitons that is proportioonal to the lateral body rates only (not spin). The rotational equations of motion now become:

$$\mathbf{I}\dot{\omega} + \omega \times \mathbf{I}\omega = \mathbf{M}_{ext} - \dot{\mathbf{I}}\omega + \dot{m}\rho_e \times \omega \times \rho_e + \rho_e \times \mathbf{T} + \mathbf{R}_{gain}\omega$$

(77)

where the $\boldsymbol{R}_{gain}$ is given by

$$\mathbf{R}_{gain} = \sum_m \left[B_m^{(r)}(-\varepsilon A_m + H_m^{(r)}) + B_m^{(i)}(D_m + F_m - H_m^{(i)}) \right],$$

(78)

assuming a velocity and pressure distribution inside the STAR48 engine based on an expansion in cylindrical Legendre functions [Flandro] given by:

23
American Institute of Aeronautics and Astronautics

$$u = \sum_m B_m Q_m \exp(\beta t)$$
$$p = \sum_m A_m \phi_m \exp(\beta t)$$

(79)

where β is a frequency in rad/s, Q_m and ϕ_m are velocity and pressure amplitudes, A_m, B_m, C_m, D_m, E_m, F_m, H_m are "gas-dynamic" mode shapes described in [Flandro], the system natural frequencies are:

$$\lambda_{kmn} = 2\left[1 + (2\pi\xi b / n)^2\right]^{-1/2}$$

(80)

the vehicle nutation frequency is:

$$\omega_0 = \Omega\left(1 - I_{spin} / I_{transverse}\right)$$

(81)

Figure 15 (left) shows the result of the verification of the model used to derive the Rgain. It was compared to the derivation of the Rgain for the Westar vehicle, which is documented in [Flandro]. While the unsteady gas dynamic model did not reproduce exactly the Westar data, the trend was very similar, including the amplification of the lateral body rates, with a discrepancy only in the peak value of the amplification. Figure 15 (right) depicts the vehicle's Rgain as a function of time, showing the distinct amplification of lateral rates during the burn. However, the resultant body torques are small, hence the model of the unsteady gas-dynamic effects predicts lateral torques (shown in Figure 16) a factor of 10 smaller than the jet damping torques.
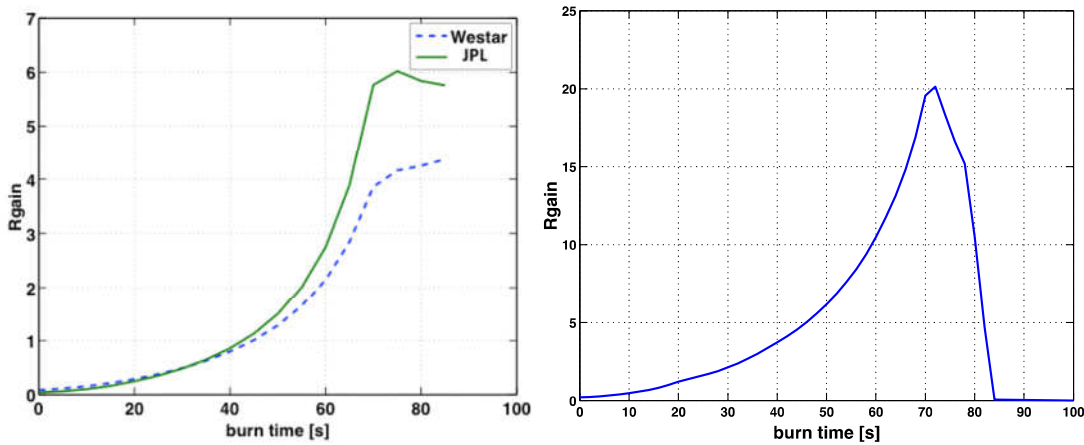
Figure 15. Rgain and Rgain torque, during burn.
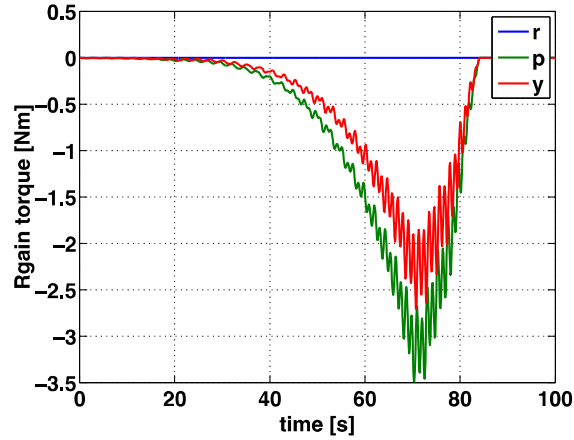
Figure 16. Rgain and Rgain torque, during burn.

IV. Visualization of LDSD Dynamics using JPL's DSENDS Flight Mechanics Engine

DSENDS is a physics-based engineering simulator for space missions developed by the Dartslab team at NASA's Jet Propulsion Laboratory[1]. DSENDS models the spacecraft as a multi-body system where the spacecraft position, attitude, articulation and body flexibility states (and their rates) interact with gravity, atmospheres, terrain, and on-board spacecraft devices in response to ground commands and flight-software directed sensing and control actions. DSENDS is a deployment of the Dshell multi-mission simulation framework. It was originally designed to provide functionality for Entry, Descent and Landing (EDL) problems but has since been generalized to provide capabilities relating to spacecraft ascent, orbit, proximity operations, rendezvous descent and surface operations (e.g. roving). The DSENDS tool is in use at JPL for technology/concept development – all the way from Pre-Phase A analysis to flight operations. It is used by NASA/JPL missions for performance studies, cross-validation of other simulations and tools, and flight-critical EDL mission operations including lander targeting. It has been used by NASA/JPL Technology Programs, Program Offices, and Mission Analysis teams as a high-fidelity simulator to support proposal development, as an integration platform and test-bed for studies, and as a tool for algorithm and software development. As part of JPL's end-to-end Mission systems, DSENDS interoperates with JPL's Interplanetary Mission design and navigation software Monte. In flight-operations it is used to verify the actions of mission actions (e.g. determine the landing footprint), perform targeting operations (e.g. to design interplanetary trajectory correction maneuvers). As the test program for LDSD is developed the various test scenarios are generated in DSENDS and displayed using the visualization capabilities of the tool[9]. This allows the test engineers to design the test system (e.g. size the rocket motors used to accelerate the test article), visualize the trajectory and related constraints (e.g. land over- flight, communication line-of-sights), camera placements, etc.

25
American Institute of Aeronautics and Astronautics

Figure 17. Snapshot of DSENDS flight simulator.

V. Conclusion

This paper derives the equations of motion of variable mass systems using a coordinate-free approach. These equations have been verified with simple models, and the terms originating in the steady and unsteady gas-dynamic interaction effects have been used in the modeling and simulation of the propulsive phase of the Supersonic Inflatable Advanced Decelerator when the vehicle is spinning. The variable mass terms have an effect both the translation and the rotation of the vehicle during thrust, indicating an increase in the roll rate. The approach used in the paper was to develop a powered phase full 6 DOF dynamic model of the SIAD test vehicle, and apply a jet damping model typically used for a variable mass rigid body slender rocket. Several authors have specialized the jet damping models to capture the interaction between the combustion physics and the system motion. In this paper we describe how these models are used for the prediction of the SIAD vehicle stability during motor burn, and address the effect of different exit gas velocity profiles on the roll spin stability during burn. The effect of thrust misalignment has been investigated and seems to be negligible. The jet damping analysis is usually based only on variable-mass rigid body model of jet-damping, which applies to slender rockets. STAR-48 is however a large rocket, and internal gas-dynamic interactions are important. STAR-48 motors are also prone to coning instability (nutation amplification due to unfavorable gas-dynamic interactions), which has been observed in flight on several occasions. To fully address this issue, the variable-mass rigid body model was extended to account for the internal unsteady gas-dynamic interaction by including modeling of the inertial waves. The conclusion was that this extended model predicts lateral torques a factor of 10 smaller than the jet damping torques. The added effect of vehicle aerodynamics on the rigid body variable mass dynamics, which is important because of mass depletion, is found not to adversely affect the static aerodynamic stability of the system by changing the center of mass to center of pressure distance. The results of the simulations show that in the absence of thrust misalignment the roll spin rate grows from 15 to 25 deg/s, depending on the assumed exit velocity profile.

Acknowledgments

References

[1]Balaram, J., Austin, J., Banerjee, P., Bentley, T., Henriquez D., Martin, B., McMahon, E., and Sohl, G.: Dsends-a high-fidelity dynamics and spacecraft simulator for entry, descent and surface landing. In Aerospace Conference Proceedings, 2002. IEEE, volume 7, pages 7–3343. IEEE, 2002.

[2]Balloon Launched Decelerator Test Program, Post Flight test Report, Viking Project, 1975, NASA report TR-3720295.. NAS1-9000.

[3]Cornelisse, J., Schoyer H., and Wakker, K.: Rocket propulsion and spaceflight dynamics. London: Pitman, 1979, 1, 1979.

[4]Eke, Wang: Equations of motion of two-phase variable mass systems with solid base, Journal Applied Mechanics ,Vol. 61, December 1994.

[5]Eke, Mao, Morris: Free Attitude Motions of a Spinning Body with Substantial Mass Loss, Journal Applied Mechanics,Vol. 71, March 2004.

[6]Eke, Tran, Sookgraev: Dynamics of a Spinning Rocket with Internal Mass Flow, Nonlinear Dynamics and Systems Theory, (6) 2, 2006, pp.129-142.

[7]Flandro, G.: Fluid Mechanics of Spinning Rockets, AL-TR-86-072, 1987.

[8]Fox, R. W., McDonald, A. T., and Pritchard, P.J.: Introduction to fluid mechanics, volume 2. John Wiley & Sons New York, 1998.

[9]Low Density Supersonic Decelerator, http://www.nasa.gov/mission_pages/tdm/ldsd/index.html#.U7XkvhbxVdA

[10]Thomson, W. T.: Equations of motion for the variable mass system. AIAA Journal, 4(4):766–768, 1966.

[11]Van der Ha, J. and Janssens, F. L.: Jet damping and misalignment effects during solid rocket motor burns, AIAA paper 2003-5328.

[12]Wang, Eke: Rotational Dynamics of Axisymmetric Variable Mass Systems, Journal Applied Mechanics,Vol. 62, December 1995.